Research Article | Vol. 26, No. 24 | 26 Nov 2018 | OPTICS EXPRESS 32332
Optics EXPRESS

Photonic molecules defined by SU-8 photoresist strips on a photonic crystal waveguide

STEPHEN A. LENNON,[1] FREDERIC S. F. BROSSARD,[2] LUKE P. NUTTALL,[1] JIANG WU,[3] JONATHAN GRIFFITHS,[4] AND ROBERT A. TAYLOR[1,*]

[1] *Clarendon Laboratory, Department of Physics, University of Oxford, Oxford OX1 3PU, UK*
[2] *Hitachi Cambridge Laboratory, Hitachi Europe Ltd, Cambridge CB3 0HE, UK*
[3] *Department of Electronic and Electrical Engineering, University College London, Torrington Place, London WC1E 7JE, UK*
[4] *Cavendish Laboratory, University of Cambridge, J. J. Thomson Avenue, Cambridge CB3 0HE, UK*
[*] *robert.taylor@physics.ox.ac.uk*

Abstract: We present experimental and numerical investigations of photonic molecules obtained from laser patterned SU-8 photoresist strips on photonic crystal waveguides. Properties of cavities defined by a single strip are investigated and we show that two adjacent strips on a waveguide form a pair of optically coupled cavities. Simulation results and micro-photoluminescence mapping measurements demonstrate that the coupling strength is tunable by controlling the separation between the strips. Confocal mapping with decoupled collection and excitation points is used to explicitly show coupling between two cavities of a photonic molecule.

1. Introduction

A system of two coupled optical cavities forms a photonic molecule (PM), so-called for the similarity of its optical modes to the bonding and anti-bonding orbitals of a diatomic molecule [1]. PMs coupled to quantum dots (QDs) have attracted significant interest for applications in the fields of quantum optics and cavity quantum-electrodynamics, including demonstrations of entangled photons [2] and ultrafast control of light-matter interactions [3]. Additionally, it has recently been shown that an unconventional photon blockade [4–6] can be achieved, which can operate with a weakly coupled emitter [7], rather than the more experimentally challenging requirement of an emitter strongly coupled to a cavity mode [8, 9].

Photonic crystal (PhC) cavities are particularly tailored to applications requiring light-matter coupling using QDs due to their high quality factor (Q), small mode volume (V) optical modes and their inherent scalability [10–12]. QD-cavity coupling is usually sought after for the achievement of efficient solid-state, on-demand single photon sources [13–15], often for applications in quantum-cryptography protocols [16] or optical quantum computing operations [17, 18]. A wide variety of PM structures can also be realized in PhC devices by placing individual cavities in close enough proximity that they can couple evanescently to each other. PMs based on L3 cavities [19–23], L5 cavities [24] or engineered defects in waveguides [25, 26] are frequently used, with coupling strength between the cavities tunable by altering the cavity separation or the PhC hole shapes and sizes [27].

Achieving coupling of a self-assembled QD to a PhC cavity mode is difficult in practice due to the random distribution of QD positions and emission wavelengths resulting from epitaxial growth. Obtaining the necessary spatial and spectral overlap of the QD emission with the cavity mode often relies on chance, with typical methods relying on a brute-force approach in which many devices are fabricated with a low yield of successful coupling [28–30]. Clearly, this is impractical for reliable production of on-chip devices containing multiple coupled dot-cavity

#346492 https://doi.org/10.1364/OE.26.032332
Journal © 2018 Received 21 Sep 2018; revised 31 Oct 2018; accepted 1 Nov 2018; published 21 Nov 2018

Optics EXPRESS

structures.

In our previous work, we demonstrated a novel technique to fabricate cavities optically by placing a disk of SU-8 negative photoresist on a photonic crystal waveguide containing embedded quantum dots [31]. The advantage of this technique is the potential to position the cavity mode to overlap with a single QD, located using micro-photoluminescence (μPL) measurements. In this work we show that a similar technique can be used to define PMs using two strips of SU-8 photoresist patterned perpendicular to the waveguide. As in our previous work [31], the approach used here is capable of locating single QDs, thus giving a deterministic way of obtaining a PM-dot coupled system. Therefore, this technique could facilitate a practical implementation of the unconventional photon blockade in a QD-PhC system in subsequent work.

We first report on an improved single cavity device design using an SU-8 strip instead of a disk to generate the optical modes, which proves to be a more reliable fabrication technique and results in a similarly high Q/V ratio that is favourable for dot-cavity coupling experiments. We then show successful fabrication and characterisation of PMs from two adjacent SU-8 strips on the PhC waveguide. We demonstrate that by altering the separation between the SU-8 strips, we can alter the coupling strength between the two resulting cavities, enabling us to observe the transition from independent, uncoupled cavities to strongly coupled PMs with delocalized optical modes. Finally, confocal mapping techniques with independent control over the excitation and collection positions enable us to probe the individual cavities of an SU-8-defined PM to show optical coupling between the two cavities explicitly.

2. Single SU-8 strip cavity modes

The placement of a small disk of SU-8 photoresist on top of a PhC membrane waveguide results in a local increase in refractive index. Even a small increase in refractive index is sufficient to generate a locally confined cavity mode with a high Q/V ratio [32]. The method for fabricating such a cavity is detailed in our previous work [31], which we have now refined to improve its reproducibility. In this work, strips of SU-8 are written perpendicular to the PhC waveguide, as seen in Fig. 1. This is similar to the inkjet printed cavity design presented in the work by Brossard et al. [33]. The main advantage of this design is that it eliminates the possibility of misalignment between the SU-8 and the waveguide, which could occur when writing SU-8 disks on the PhC. Misalignment between the SU-8 disk and waveguide was found to reduce the reproducibility of the cavities and in some instances was found to reduce the Q of successfully fabricated cavity modes.

Finite-difference time-domain (FDTD) simulations were performed using Lumerical FDTD Solutions software [34] to model a PhC waveguide in a 200 nm-thick GaAs membrane with refractive index $n = 3.33$ [35]. The waveguide is formed along the x-direction from a missing row of holes in a triangular PhC lattice with a lattice spacing of $a = 340$ nm and hole radius $r = 0.27a$. Simulated cavity mode parameters for a 1 μm-wide SU-8 strip (to match the size of the focused laser spot of the μPL system) with refractive index 1.57 [36] on top of the PhC waveguide are presented in Fig. 2(a). The SU-8 strip spans the extent of the PhC in the y-direction, perpendicular to the waveguide. Values of the quality factor and mode volume are presented for a range of strip thicknesses from 50–550 nm. In addition to the total quality factor, Q_{total}, the in-plane and out-of-plane components, Q_{in} and Q_{out} respectively, are calculated. In similarity to our previous cavity design defined by an SU-8 disk, we observe that Q_{total} is limited by Q_{in}, which is much smaller than Q_{out} due to coupling of the confined TE-like mode to leaky TM-like modes, facilitated by the broken z-symmetry of the structure [37]. The calculated quality factors for the SU-8 strip cavity are marginally lower than those of the SU-8 disk cavities, but this is offset by the smaller mode volume of the SU-8 strip cavities, which results in a similarly high Q/V ratio as is favourable for Purcell enhancement. The calculated values of Q_{total}/V are presented in Fig. 2(a).

We note that potential infiltration of the PhC holes with SU-8 beneath the strip is not expected to

Optics EXPRESS

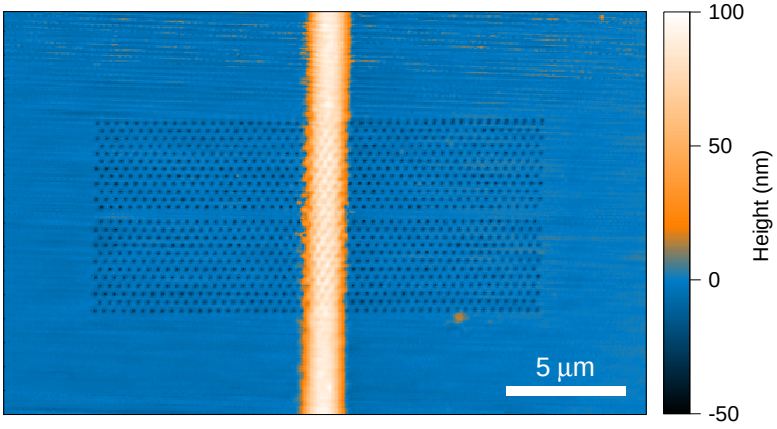

Fig. 1. AFM image of an SU-8 strip PhC waveguide cavity with a mean thickness of 90 nm over the PhC and a Q of 7400.

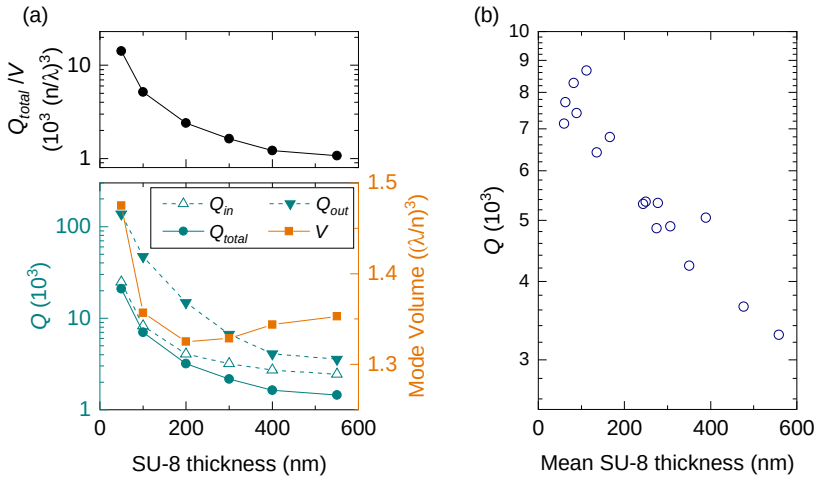

Fig. 2. (a) FDTD simulation results for a 1 µm-wide SU-8 strip on a PhC waveguide. The width of the waveguide, defined as the separation between the centres of the two rows of holes either side of the waveguide, is given by $W = 0.98\sqrt{3}a$. (b) Experimental data obtained from a batch of successful SU-8 strip cavities. Q values were measured by µPL measurements and the mean SU-8 strip thickness has been extracted from AFM measurements of each device via profile averaging across the extent of the PhC.

have a detrimental effect on the cavity mode properties: a simulation of a 1 µm-wide, 100 nm-thick strip, with PhC holes completely covered by the strip filled in with SU-8 (across the 200 nm depth of the membrane), yielded $Q = 7860$ and $V = 1.20\,(\lambda/n)^3$, compared to values of $Q = 7020$ and $V = 1.36\,(\lambda/n)^3$ for unfilled holes. This suggests that if SU-8 infiltration occurs – which is difficult to determine in practice – it is unlikely to be a problem, which is in agreement with similar investigations into the effect of hole infiltration in PhC cavities [38]. In fact, SU-8 infiltration may prove beneficial for the cavity modes, increasing the Q/V ratio.

Devices were fabricated on a GaAs chip with embedded high density self-assembled InGaAs

Optics EXPRESS

QDs (~100 dots/μm^2) to allow study of the SU-8 strip cavities using μPL techniques. The PhC waveguides were patterned onto a coating of poly(methyl methacrylate) using a 100kV VB6 Leica e-beam machine and reactive ion etching was used to transfer the design to the substrate. Suspended PhC membranes were produced by selectively etching away an underlying sacrificial AlGaAs layer using 32% HCl treatment. A more detailed description of the fabrication process can be found in the work by Brossard et al. [11]. The PhC lattice constant and hole size were tailored to produce cavity modes in the optical telecommunications O-band.

The sample was spin-coated with SU-8 photoresist solution, prepared as stated in our previous work [31] with some minor adjustments. A ratio of 1 part SU-8 2007 diluted in 7 parts cyclopentanone was used, which results in a more concentrated solution than previously used. This, together with the addition of an extra spin phase, was designed to improve the reliability of the SU-8 adhesion to the sample surface. The additional spin phase was a slow initial spin at 500 rpm with an angular acceleration of 200 rpm/s before spinning the sample at 2800 rpm. SU-8 strips were exposed over the PhCs using a 405 nm laser diode with a power of 17.5 μW at the output of the 100 × magnification, 0.5 NA microscope objective. The objective, which was mounted on a piezo-actuated 3-axis translation stage with 0.3 nm resolution, was moved to write the strip perpendicular to the waveguide. The writing speed was chosen in the range 0.125 μm/s to 1 μm/s to control the exposure dose and therefore the thickness of the SU-8 strip.

Micro-photoluminescence mapping measurements taken before and after writing the SU-8 lines were compared to confirm the creation of new cavity modes. This comparison process is described in more detail in our previous work [31] – the single SU-8 strip cavities showed clear evidence of the creation of new cavity modes after writing them, similar to the SU-8 disk cavities. Photoexcitation above the band gap was provided by a He-Ne continuous wave laser (632.8 nm) focused to a ~1 μm diameter laser spot through the same objective used for SU-8 exposure, with a power of ~10 μW after the objective. The sample was mounted in a continuous flow liquid helium cryostat, which was cooled down to 8 K. Photoluminescence from the sample was collected by the objective and directed through a 0.3 m spectrometer onto a 1024 pixel, liquid nitrogen-cooled (−100 °C) InGaAs array. The maximum effective resolution of the spectrometer was 0.03 nm at 1280 nm, defined from one pixel width. The maximum resolution was used for Q measurements; a grating with a lower resolution of 0.1 nm at 1280 nm was used for μPL mapping measurements in this work.

Data collected from the SU-8 strip cavities are presented in Fig. 2(b). The mean thickness of the SU-8 strip over the extent of the PhC was extracted from atomic force microscope (AFM) measurements of each device. As can be seen from the AFM image in Fig. 1, the SU-8 strips are highly uniform over the PhC. Profile averaging was performed to extract the mean profile of the SU-8 strip, which was fitted with an inverse polynomial to obtain the mean SU-8 thickness presented against Q in Fig. 2(b). We observe that Q values of up to 8600 are achievable, which exceeds the maximum value of 7000 reported for SU-8 disk cavities in our previous work. A trend of higher Q for thinner SU-8 strips is clearly observed, matching predictions from the FDTD simulations presented in Fig. 2(a).

3. Modeling SU-8 strip photonic molecules

By placing two SU-8 strips on a single PhC waveguide, it is possible to create two distinct cavities. If the SU-8 strips are in close enough proximity, the modes of the individual cavities can become optically coupled and we observe the formation of supermodes attributed to a PM. In these simulations, we focus on the two lowest energy modes of the system, which follow symmetric (S) and antisymmetric (AS) boundary conditions for the fields about $x = 0$ [as shown in Fig. 3(a)]. In all cases simulated, the S mode constituted the lowest energy mode. In the case of a strongly coupled PM, the modes form S and AS supermodes, arising from the in-phase and out-of-phase oscillations of the constituent cavity modes [1]. The simulated E_y field profile of

Optics EXPRESS

the S and AS supermodes expected in an SU-8 strip PM with a strip separation of 2 µm is shown in Fig. 3(a). The observation of such a mode is only possible when the coupling strength, J, between the two cavities is sufficiently high and the cavity detuning, $\Delta\lambda$, between the two cavities is sufficiently small. The cavity detuning refers to the difference in resonant wavelength of the isolated individual cavities; a large detuning will result in modes more localized in the individual cavities, rather than the highly delocalized modes seen in a strongly coupled PM [26]. Therefore, the task of realizing a strongly coupled PM experimentally is a good test of the uniformity of our SU-8 strip cavities.

The S and AS modes of a PM are expected to exhibit an energy splitting, as predicted by coupled mode theory [39]. For two uncoupled cavity modes with equal linewidths and finite cavity detuning $\Delta\lambda$, the mode splitting, $\Delta\Omega$, induced by a coupling strength J between them is given by:

$$\Delta\Omega = \sqrt{(\Delta\lambda)^2 + 4J^2} \tag{1}$$

and in the case of zero detuning ($\Delta\lambda = 0$), the mode splitting is given by $\Delta\Omega = 2J$. FDTD simulation results for SU-8 PMs of varying strip separation with zero detuning are presented in Fig. 3(b). The results predict a reduction in coupling strength (equal to half the mode splitting) as the strip separation is increased, as would be expected from the reduced evanescent field overlap of the individual cavity modes.

To further characterise the PMs, we computed the PM mode profiles that we expect to observe using our µPL mapping system. The mode profiles were calculated by convolving the squared magnitude of the time-averaged electric field profile along the centre of the waveguide with a 1 µm Gaussian to represent the excitation spot. The resulting AS mode profile always contains two peaks [similar to the M2 mode profile in Fig. 5(c)] which are spaced sufficiently far apart to be resolved by the system (we note that at larger strip separations, the S mode is also predicted to have two resolvable peaks localized at the strip positions). We define the AS peak separation

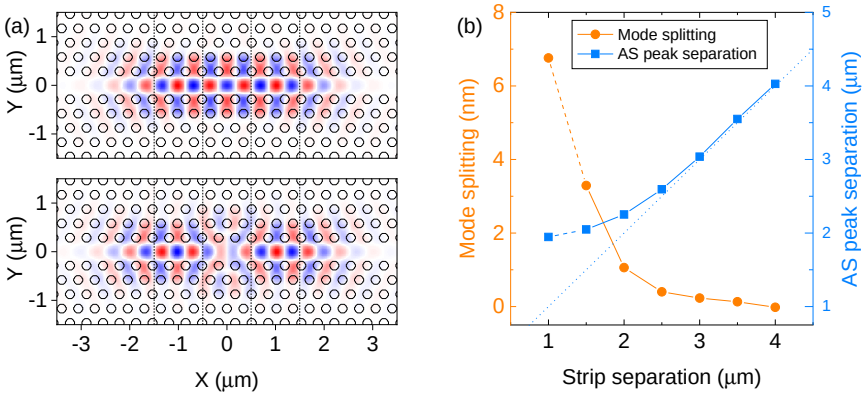

Fig. 3. FDTD simulation results of SU-8 strip PMs with 100 nm-thick, 1 µm-wide strips. (a) E_y field profile of the S (top) and AS (bottom) modes with an SU-8 strip separation of 2 µm (centre-to-centre). Red and blue represent opposite polarities of the field and the dotted lines show the positions of the SU-8 strips over the PhC. (b) Calculated wavelength splitting between the S and AS mode and spatial separation between the two peaks of the AS mode (when convolved with a 1 µm Gaussian) as a function of SU-8 strip separation. The dashed blue line is to guide the eye, indicating strip separation equal to AS peak separation. A strip separation of 1 µm corresponds to a single SU-8 strip of 2 µm width.

Optics EXPRESS

as the centre-to-centre distance of the two peaks, which can be compared to experimental μPL mapping results to help verify that the SU-8 PMs have been fabricated successfully. As shown in Fig. 3(b), at large strip separations (around 4 μm) the AS peak separation matches the strip separation, as the peaks of the mode are highly localized at the cavity positions. The mode splitting tends to zero, indicating that the coupling strength is small and coupling would be lost in a physical system with non-zero detuning, resulting in uncoupled or very weakly coupled cavities with highly localized modes. As the strip separation is reduced, the increased coupling strength is signified by an increased mode splitting and also an increase in the AS peak separation beyond the separation of the SU-8 strips. For short separations, the system gradually evolves from a PM to a single cavity, which is characterized by its large mode splitting and significant divergence of the AS peak separation away from the line of equality with strip separation. Data for a 2 μm-wide single SU-8 strip cavity are shown, which is equivalent to a strip separation of 1 μm. Evidently, for a single cavity, the AS peak separation becomes comparable to the size of the 2 μm-wide single strip.

The FDTD results in Fig. 3(b) demonstrate the ability to control the coupling strength of the PM by altering the SU-8 strip separation. This enables a degree of control over the mode splitting with little detrimental impact on the Q of the cavity modes, which simulation results showed to be greater than 4900 (indicating linewidths of ~0.26 nm or narrower) for all S and AS modes tested. This is comparable to the Q of 7000 calculated for a 2 μm-wide SU-8 strip single cavity [we note that these Q factors are expected to increase as the strip thickness is reduced, as in Fig. 2(a)]. The ability to choose the strip separation and therefore determine the mode splitting using post-fabrication μPL techniques makes this method promising for applications that rely on matching the mode splitting to an experimentally measured system, such as coupling the PM modes to multiple excitonic transitions of a QD [2].

4. μPL mapping of SU-8 strip PMs

A batch of double SU-8 strip devices was written on a sample with the same characteristics as outlined in section 2, using the same SU-8 processing techniques. Two strips were written on each device with a separation along the waveguide ranging from 1 μm to 5 μm in 0.5 μm increments. An example with a strip separation of 2.5 μm is shown in Fig. 4. The writing speed was varied between 0.25 μm/s and 0.5 μm/s to control the SU-8 strip thickness; the exposure parameters were selected to guarantee reliable fabrication rather than the thinnest possible, highest Q factor SU-8 strips. Consequently, Q factors were typically between 3500-5500. μPL maps at 8 K were performed before and after writing the SU-8 strips to confirm the creation of new cavity modes. For each device, the laser spot was moved along the waveguide in 0.2 μm steps in order to map out the mode profiles [26]. Movement of the laser spot was enabled by piezo-controlled movement of the microscope objective. A power of ~50 μW after the objective was used for mapping.

Figure 5 shows some selected examples of μPL maps from devices with a range of strip separations. The behaviour of the two lowest energy modes, which we call M1 and M2, demonstrates evidence of increased coupling between the cavities as the strip separation is reduced. At a large separation of 4.5 μm [Fig. 5(a), device D1] two independent, highly-localized cavity modes are observed corresponding to two uncoupled cavities. In this case, the wavelength splitting between the two modes is dominated by the cavity detuning. The most likely source of this detuning is from fabrication inconsistencies; imperfections in the photonic crystal and variation in the SU-8 strip geometry and dimensions result in shifts in the cavity emission wavelength. In Fig. 5(b) (strip separation 3.5 μm, device D2) the two cavities are evidently coupled, with a moderate degree of mode delocalization. The presence of cavity detuning prevents fully delocalized supermodes: previous work on a similar coupled cavity system has demonstrated that the smaller the ratio of $J/\Delta\lambda$, the more localized towards the individual cavities the modes are [26]. A high degree of mode delocalization is evident for the device in Fig. 5(c)

Optics EXPRESS

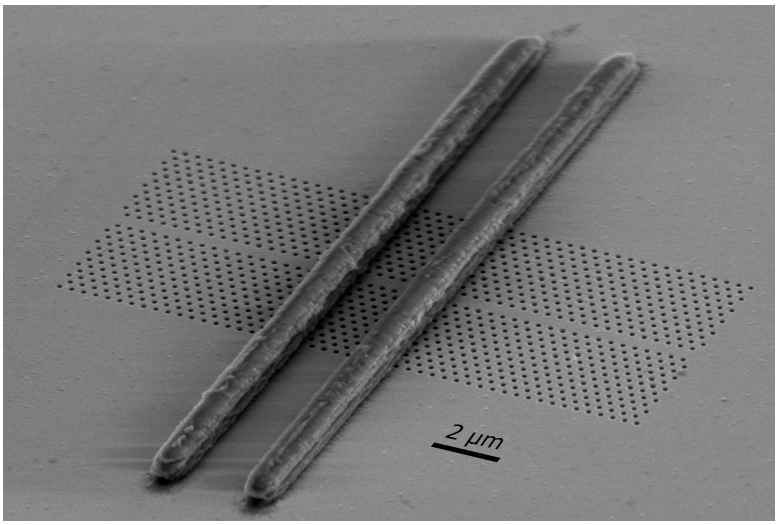

Fig. 4. Scanning electron microscope image of two SU-8 strips written on a PhC waveguide at a separation of 2.5 μm. The mean thickness of the strips was determined from AFM measurements to be 0.55 μm, obtained by averaging the thickness of the strips over the width of the PhC.

(strip separation 2.5 μm, device D3), for which the characteristic S and AS supermodes are observed. This shows evidence of a strongly coupled PM with large coupling strength relative to the detuning. An AFM image of the same device is provided in Fig. 5(d).

We further characterize the PMs by measuring the delocalization of the M2 mode, which enables the cavity detuning and the coupling strength to be estimated. From coupled mode theory, the modes of the coupled system, $\Psi_+(\boldsymbol{r})$ and $\Psi_-(\boldsymbol{r})$, are given by linear combinations of the isolated cavity modes, $\psi_1(\boldsymbol{r})$ and $\psi_2(\boldsymbol{r})$:

$$\Psi_+(\boldsymbol{r}) = \left(\sin\frac{\theta}{2}\right)\psi_2(\boldsymbol{r}) + \left(\cos\frac{\theta}{2}\right)\psi_1(\boldsymbol{r}) \tag{2}$$

$$\Psi_-(\boldsymbol{r}) = \left(\cos\frac{\theta}{2}\right)\psi_2(\boldsymbol{r}) - \left(\sin\frac{\theta}{2}\right)\psi_1(\boldsymbol{r}) \tag{3}$$

$$\tan\theta = 2J/\Delta\lambda \tag{4}$$

where θ is a weighting factor. The delocalization factor, F, of a given mode is defined as the ratio of the electric field energy at the centres of the two cavities of the PM. It is always defined as the lowest divided by the highest of the two field energies. Assuming that the isolated cavities have relatively well confined modes, cross-terms can be neglected from Eqs. (2)–(3) and the delocalization factor is given by [26]:

$$F = \frac{\sin^2(\theta/2)}{\cos^2(\theta/2)} = \tan^2(\theta/2) \tag{5}$$

hence the delocalization factor is dependent on the ratio $J/\Delta\lambda$, related to θ by Eq. (4). For an ideal PM with identical cavities and zero detuning, the M2 peaks will correspond to AS supermode peaks with equal amplitude and therefore F will have its maximum value of 1. For finite detuning, F decreases as the ratio of coupling strength to detuning decreases, which predicts

Optics EXPRESS

a mode profile increasingly localized towards one of the individual cavities. We estimated the delocalization factors of the measured M2 modes by calculating the amplitude of the dimmest peak divided by the amplitude of the brightest peak. The measured F values of coupled cavity devices D2 and D3 were 0.33 and 0.77 respectively, while the uncoupled cavities of D1 yield an F value of less than 0.01. These observations are consistent with expectations from Eq. (5): as the separation is increased, the decrease in coupling strength results in a lower $J/\Delta\lambda$ ratio, which yields a decrease in F. By rearranging Eq. (4) for θ and substituting into Eq. (5), it can be shown that the $J/\Delta\lambda$ ratio is related to F by:

$$\frac{J}{\Delta\lambda} = \frac{\sqrt{F}}{1-F} \tag{6}$$

which, combined with Eq. (1), enables J and $\Delta\lambda$ to be estimated from the measured values of F and $\Delta\Omega$:

$$J = \left(\frac{\sqrt{F}}{1+F}\right)\Delta\Omega \tag{7}$$

$$\Delta\lambda = \left(\frac{1-F}{1+F}\right)\Delta\Omega \tag{8}$$

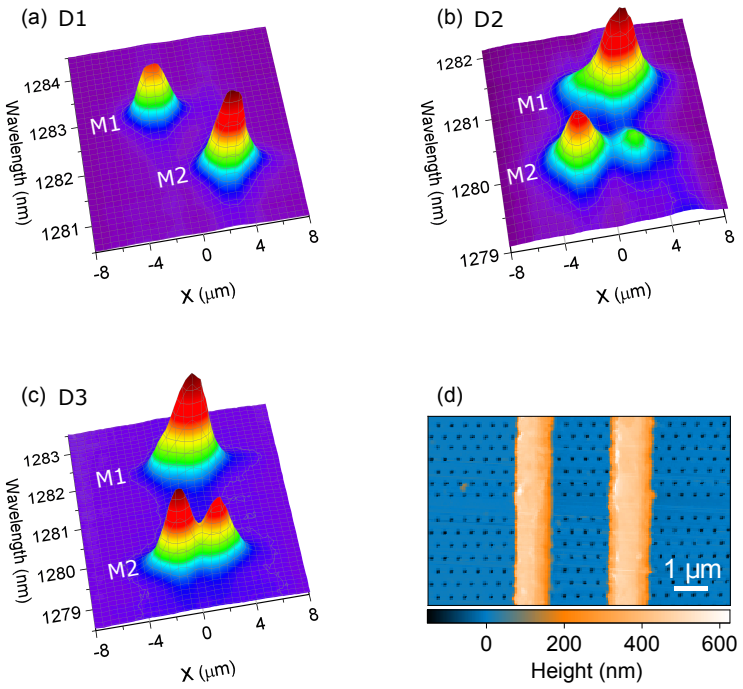

Fig. 5. (a)–(c) μPL maps from selected SU-8 double strip devices, showing increasing coupling as the strip separation is reduced. (a) Device D1, separation 4.5 μm. (b) Device D2, separation 3.5 μm. (c) Device D3, separation 2.5 μm. Devices D1, D2 and D3 show uncoupled, coupled and strongly coupled cavity modes respectively. (d) AFM image of device D3. Note that the full size of the holes in the PhC is not resolved by the AFM tip, so they appear smaller than their true size.

Optics EXPRESS

For devices D2 and D3 we estimate coupling strengths of $J_{D2} \sim 0.4$ nm and $J_{D3} \sim 1.1$ nm from mode splittings of 0.97 nm and 2.33 nm, respectively. The estimated detunings of the devices are $\Delta\lambda_{D2} \sim 0.5$ nm and $\Delta\lambda_{D3} \sim 0.3$ nm and we estimate a detuning of $\Delta\lambda_{D1} = 1.27$ nm from the mode splitting of the uncoupled cavities of D1. The differences in the detuning values are anticipated to result predominantly from random variation of the disorder-induced detuning caused by e-beam fabrication imperfections, although minor fluctuations of the SU-8 strip thickness may also contribute. We note that the strongly coupled device D3 in particular is predicted to have a high coupling strength and small detuning, which correlates with its highly delocalized AS supermode.

Experimental data from a large batch of 87 devices were collected for comparison with the FDTD simulation results presented in Fig. 3(b). The mean mode splitting between the M1 and M2 modes for each SU-8 strip separation is presented in Fig. 6(a). The data match the trend predicted by the FDTD results well, except for the additional effects of fabrication imperfection-induced cavity detuning not accounted for in the simulation. Instead of converging to zero as in the zero detuning case, Eq. (1) predicts that the mean mode splitting should converge towards the mean value of $\Delta\lambda$ (which is expected to be independent of the strip separation) as the strip separation is increased and J tends to zero. At large separations, the cavity detuning is expected to be the sole source of the mode splitting. Therefore, we estimate a mean cavity detuning of $\overline{\Delta\lambda} = (1.15 \pm 0.13)$ nm from the mode splitting of the PMs with a strip separation of 4 µm or more. The magnitude of this detuning is comparable to e-beam defined PhC PMs reported in the literature [20, 21, 26, 27], which supports our novel SU-8 writing technique as a reliable method for creating PMs and suggests that the additional photolithography step is not a significant source of cavity detuning beyond the PhC fabrication imperfections.

The mean peak spacing for each strip separation is shown in Fig. 6(a), which was measured as an analogue to the AS peak spacing defined in section 3. Due to the presence of cavity detuning that was not accounted for in the FDTD simulations, it was not always possible to measure the AS peak separation in practice. In the case of a high $J/\Delta\lambda$ ratio, the M2 mode is highly delocalized and contains two resolvable peaks (such as for devices D2 and D3), from which the centre-to-centre peak separation can be measured and is equivalent to the AS peak spacing. However, for a low $J/\Delta\lambda$ ratio, the M2 mode may only have one clear peak (such as for device D1). In this case the peak spacing is defined as the separation of the M1 and M2 peaks. We observe that the peak spacing converges towards the strip separation at large separations (corresponding to the cavity positions), for which the inter-cavity coupling is weak. This matches expectations of the AS peak separation from the simulation results and we see a comparable trend: as the strip separation is reduced and the coupling strength increases, the peak spacing becomes larger than the strip separation. A single cavity is formed for a 1 µm strip separation.

To verify the trend in coupling strength with strip separation experimentally, we applied two different methods to estimate variation of the mean coupling strength with strip separation for the whole batch of devices. In method A, the coupling strength was calculated independently for each device from the measured $\Delta\Omega$ and F values using Eq. (7). The mean coupling strength was then calculated from devices with the same strip separation, which is presented in Fig. 6(b). Also shown are the mean coupling strengths estimated via method B, in which the mean mode splitting from Fig. 6(a) is used with the estimated mean detuning, $\overline{\Delta\lambda} = 1.15$ nm, to calculate the coupling strength using Eq. (1). We note that method B cannot be used to estimate J for individual devices like method A, since the disorder-induced detuning can vary significantly from cavity to cavity and $\overline{\Delta\lambda}$ often does not accurately represent the detuning of a single device. Therefore method B can only be used to estimate the mean values of J at each separation, assuming that the mean detuning is independent of strip separation. We observe that the two methods give consistent results within error and both confirm the expected trend of decreasing coupling strength with increasing strip separation. For a given cavity separation, we found

Optics EXPRESS

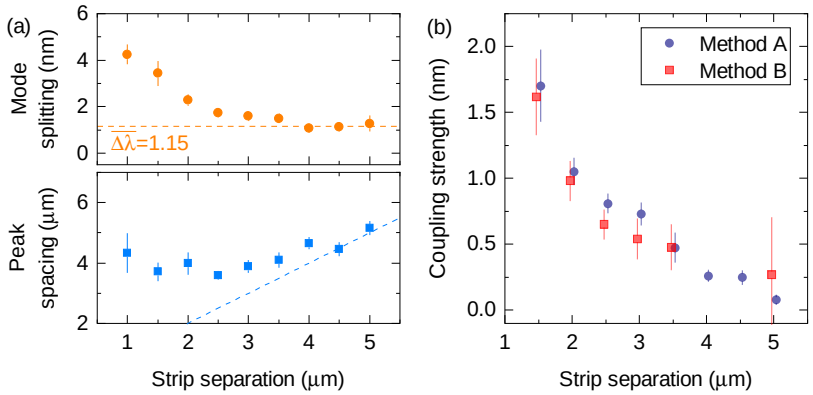

Fig. 6. (a) Mean values of mode splitting and peak spacing for each SU-8 strip separation in a batch of successful devices. Error bars represent estimates of the standard error of the mean at each separation. The dashed orange line represents the estimated mean detuning $\overline{\Delta\lambda}$ = 1.15 nm and the dashed blue line represents equality of strip separation to peak spacing, included to guide the eye. (b) Estimated mean coupling strength as a function of SU-8 strip separation, calculated using two different methods. Method A calculates the coupling strength of each individual device using the measured $\Delta\Omega$ and F before taking the mean, whereas method B uses the mean mode splitting at each separation and the estimated mean detuning $\overline{\Delta\lambda}$ from (a). Note that the datapoints have a small artificial horizontal offset either side of the true strip separation for ease of reading; the strip separations are the same as in (a). The mean coupling strength cannot be calculated for some separations using method B because the mean mode splitting is smaller than $\overline{\Delta\lambda}$. Error bars for method A represent the standard error of the mean and for method B the errors are propagated appropriately from the parameters used.

the magnitude of the estimated mean coupling strength to be comparable to other photonic crystal-based PMs in the literature [19–21], especially when compared to devices operating at a similar wavelength to the SU-8 PMs presented [22, 26]. We note that the accuracy of method A could potentially be improved by using confocal collection techniques in subsequent work, as the reduced light collection area may improve estimates of F obtained from μPL mapping of the M2 mode. However, since method B predicts the mean coupling strength independently of the measured F values, the close agreement between methods A and B supports the effectiveness of the measurements of F obtained in this work.

Both methods A and B rely on the approximation that the linewidths of the two cavities of an SU-8 PM would be equal in the absence of coupling. From AFM characterization across a representative sample of 37 devices, we found on average only 5% variation in thickness between the two strips of the SU-8 PMs. Since the Q factor of a single strip cavity mode is highly correlated with the SU-8 thickness, we deduce it is a reasonable assumption that the uncoupled cavity modes have approximately equal linewidths. We note that since the SU-8 strips were optimised for reliable fabrication rather than high Q factor, the resulting batch of SU-8 strips was moderately thick: the median strip thickness from the representative sample was 0.25 μm.

5. Confocal mapping of an SU-8 strip PM

To directly show coupling between two cavities of an SU-8 strip PM, a system was implemented to enable the cavities to be excited and collected from independently. A piezo motor actuated mirror, in combination with a telecentric 4f lens system, was used to enable independent movement of the He-Ne laser spot from the collection area, the latter being controlled by the piezo stage-mounted

Optics EXPRESS

microscope objective. For this experiment, light collected by the objective was focused through a multi-mode fibre to achieve a confocal collection area of ~2.2 µm FWHM. We examined the double-peaked M2 mode of a PM with a strip separation of 3 µm and a peak spacing of 3.3 µm – sufficiently far apart to enable us to probe the two cavities independently. From these confocal measurements, we estimate a coupling strength $J \sim 0.5$ nm and cavity detuning $\Delta\lambda \sim 0.5$ nm using the mode splitting of 1.14 nm and $F = 0.36$ obtained for this device.

In Fig. 7(a), the confocal map obtained by scanning the microscope objective is shown. In this map, the overlapping excitation and collection areas were moved simultaneously, giving the full profile of the mode. The two peaks of the M2 mode are in close proximity to the SU-8 strips, which are labelled as cavities A and B. The significant difference in intensity between the two peaks arises from localization of the mode towards B due to detuning. Figures 7(b) and 7(c) show the resulting maps when moving the excitation independently of the collection area. In this configuration, the collection is fixed over one cavity and the He-Ne laser spot is moved. As the confocal light collection area is sufficiently small to exclude light emitted by the adjacent cavity of the PM, we only expect to observe light emitted by the cavity over which the collection is centred. Coupling between the two cavities of the PM is proven by the presence of an intensity peak at the collection cavity when the excitation spot is positioned at the opposite cavity. This is confirmed for fixed collection at either cavity. The ability to independently probe the cavities with this technique could prove beneficial for experimental implementations of the unconventional photon blockade, such as exciting one cavity of the PM and observing antibunched photons from the non-pumped cavity [6]. This individual probing was not possible using the µPL mapping technique in section 4, which collected light from both cavities at once due to a large, non-confocal collection area.

The possibility of insufficient light exclusion by the confocal collection area may be a concern, as it could result in unwanted light being collected from the adjacent cavity. The advantage of investigating a PM with a moderately low F is that information from the relative intensity of the two M2 mode peaks can be used to demonstrate that the light isolation is sufficient. We observe that the intensity of the two peaks when collecting at cavity A in Fig. 7(b) is consistent with the (lower) intensity of peak A in the objective map. Similarly, the intensity of the two peaks when collecting at cavity B in Fig. 7(c) is consistent with the (higher) intensity of peak B in the objective map. This provides strong evidence that the confocal technique adequately excludes light from the adjacent cavity, resulting in collection from one cavity only. Therefore, we are confident that these confocal mapping measurements show coupling between the two cavities of the PM explicitly. We note that for an optimised PM geometry with thinner SU-8 strips, the increased Q and evanescent field overlap (from a larger mode volume) should enable stronger coupling at larger distances, which would benefit the confocal collection technique by further guaranteeing adequate exclusion of light from adjacent cavities.

6. Conclusion

In summary, we have demonstrated successfully the benefits of fabricating single cavities using a strip of SU-8 on a PhC waveguide (compared to the SU-8 disk cavity presented in our previous work [31]) and shown that these cavities have sufficient reproducibility to create PMs from adjacent strips on the same waveguide. The SU-8 strip single cavity design yielded Q values of up to 8600, with improved fabrication reliability due to less stringent conditions on the alignment of the photoresist with the waveguide. We have shown using µPL mapping techniques that PMs formed from two adjacent SU-8 strips on a waveguide have adjustable coupling strength according to the distance between the two strips. The ability to write the SU-8 strips using photolithography techniques in the same µPL system used for measurements offers the potential to position the strips to overlap with single QDs (located via photoluminescence), making the technique promising for coupling a QD to a PM. The potential for deterministic PM-dot coupling offers additional

Optics EXPRESS

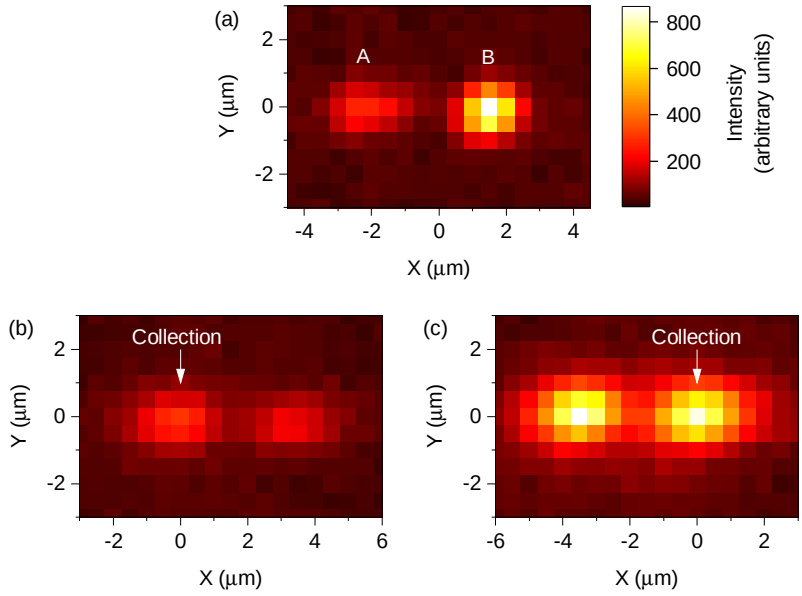

Fig. 7. Confocal µPL maps of the M2 mode of an SU-8 PM device with a strip separation of 3 µm, recorded at a wavelength of 1281.3 nm. All maps use the same colour scale for intensity. (a) Objective map showing local maxima of the mode labelled as A and B, corresponding to the two cavities of the PM. The collection and excitation are scanned simultaneously. (b) and (c): scanning mirror maps with collection fixed at peak A or B maxima respectively. The laser excitation spot is scanned independently of the collection area, from an origin $(0, 0)$ which coincides with the position of the collection area.

advantages over those addressed in our previous work relevant to single cavity-dot coupling with this technique. The ability to alter the strip separation to tune the coupling strength and mode properties, in a manner not easily possible with a single cavity, holds promise for coupling a PM simultaneously to two excitonic transitions, which could help achieve a Purcell-enhanced source of entangled photons [2]. Additionally, the challenging experimental requirement of a strongly coupled emitter needed to achieve a photon blockade in a single cavity-dot system is potentially alleviated by the unconventional photon blockade in a PM-dot coupled system, which would require only weak coupling [4–6].

As part of an investigation into a large batch of devices, trends in the mode splitting and peak spacing of the PMs were observed and shown to agree well with results from FDTD simulations. Measurements of the delocalization factor and mode splitting enabled the coupling strength and cavity detuning of individual PM devices to be estimated. Finally, a confocal mapping technique with independently movable excitation and collection areas – with resolution exceeding the strip separation – was used to probe individual cavities of a PM to prove optical coupling between them.

Data for the figures can be downloaded at: https://doi.org/10.5287/bodleian:Mz6Pp1Gz0

Funding

Engineering and Physical Sciences Research Council (EPSRC) (EP/K014978/1); Hitachi Cambridge Laboratory.

Optics EXPRESS

References

1. M. Bayer, T. Gutbrod, J. P. Reithmaier, A. Forchel, T. L. Reinecke, P. A. Knipp, A. A. Dremin, and V. D. Kulakovskii, "Optical Modes in Photonic Molecules," Phys. Rev. Lett. **81**(12), 2582–2585 (1998).
2. A. Dousse, J. Suffczynski, A. Beveratos, O. Krebs, A. Lemaitre, I. Sagnes, J. Bloch, P. Voisin, and P. Senellart, "Ultrabright source of entangled photon pairs," Nature **466**(7303), 217–220 (2010).
3. R. Bose, T. Cai, K. R. Choudhury, G. S. Solomon, and E. Waks, "All-optical coherent control of vacuum Rabi oscillations," Nat Phot. **8**(11), 858–864 (2014).
4. T. C. H. Liew and V. Savona, "Single Photons from Coupled Quantum Modes," Phys. Rev. Lett. **104**(18), 183601 (2010).
5. H. Flayac and V. Savona, "Unconventional photon blockade," Phys. Rev. A **96**(5), 53810 (2017).
6. M. Bamba and C. Ciuti, "Counter-polarized single-photon generation from the auxiliary cavity of a weakly nonlinear photonic molecule," Appl. Phys. Lett. **99**(17), 171111 (2011).
7. H. J. Snijders, J. A. Frey, J. Norman, H. Flayac, V. Savona, A. C. Gossard, J. E. Bowers, M. P. van Exter, D. Bouwmeester, and W. Löffler, "Observation of the Unconventional Photon Blockade," Phys. Rev. Lett. **121**(4), 43601 (2018).
8. A. Faraon, I. Fushman, D. Englund, N. Stoltz, P. Petroff, and J. Vučković, "Coherent generation of non-classical light on a chip via photon-induced tunnelling and blockade," Nat. Phys. **4**(11), 859–863 (2008).
9. K. M. Birnbaum, A. Boca, R. Miller, A. D. Boozer, T. E. Northup, and H. J. Kimble, "Photon blockade in an optical cavity with one trapped atom," Nature **436**(7047), 87–90 (2005).
10. J. Vučković, M. Lončar, H. Mabuchi, and A. Scherer, "Design of photonic crystal microcavities for cavity QED," Phys. Rev. E **65**(1), 16608 (2001).
11. F. S. F. Brossard, X. L. Xu, D. A. Williams, M. Hadjipanayi, M. Hugues, M. Hopkinson, X. Wang, and R. A. Taylor, "Strongly coupled single quantum dot in a photonic crystal waveguide cavity," Appl. Phys. Lett. **97**(11), 111101 (2010).
12. K. Hennessy, A. Badolato, M. Winger, D. Gerace, M. Atature, S. Gulde, S. Falt, E. L. Hu, and A. Imamoglu, "Quantum nature of a strongly coupled single quantum dot-cavity system," Nature **445**(7130), 896–899 (2007).
13. D. Englund, D. Fattal, E. Waks, G. Solomon, B. Zhang, T. Nakaoka, Y. Arakawa, Y. Yamamoto, and J. Vučković, "Controlling the Spontaneous Emission Rate of Single Quantum Dots in a Two-Dimensional Photonic Crystal," Phys. Rev. Lett. **95**(1), 13904 (2005).
14. S. Laurent, S. Varoutsis, L. Le Gratiet, A. Lemaître, I. Sagnes, F. Raineri, A. Levenson, I. Robert-Philip, and I. Abram, "Indistinguishable single photons from a single-quantum dot in a two-dimensional photonic crystal cavity," Appl. Phys. Lett. **87**(16), 163107 (2005).
15. W.-H. Chang, W.-Y. Chen, H.-S. Chang, T.-P. Hsieh, J.-I. Chyi, and T.-M. Hsu, "Efficient Single-Photon Sources Based on Low-Density Quantum Dots in Photonic-Crystal Nanocavities," Phys. Rev. Lett. **96**(11), 117401 (2006).
16. C. H. Bennett and G. Brassard, "Quantum Cryptography: Public Key Distribution and Coin Tossing," in Proc. IEEE International Conference on Computers Systems and Signal Processing (IEEE, 1984), pp. 175–179.
17. E. Knill, R. Laflamme, and G. J. Milburn, "A scheme for efficient quantum computation with linear optics," Nature **409**(6816), 46–52 (2001).
18. O. Gazzano, M. P. Almeida, A. K. Nowak, S. L. Portalupi, A. Lemaître, I. Sagnes, A. G. White, and P. Senellart, "Entangling Quantum-Logic Gate Operated with an Ultrabright Semiconductor Single-Photon Source," Phys. Rev. Lett. **110**(25), 250501 (2013).
19. K. A. Atlasov, K. F. Karlsson, A. Rudra, B. Dwir, and E. Kapon, "Wavelength and loss splitting in directly coupled photonic-crystal defect microcavities," Opt. Express **16**(20), 16255–16264 (2008).
20. S. Kapfinger, T. Reichert, S. Lichtmannecker, K. Muller, J. J. Finley, A. Wixforth, M. Kaniber, and H. J. Krenner, "Dynamic acousto-optic control of a strongly coupled photonic molecule," Nat. Commun. **6**, 8540 (2015).
21. A. Majumdar, A. Rundquist, M. Bajcsy, and J. Vučković, "Cavity quantum electrodynamics with a single quantum dot coupled to a photonic molecule," Phys. Rev. B **86**(4), 45315 (2012).
22. A. Y. Piggott, K. G. Lagoudakis, T. Sarmiento, M. Bajcsy, G. Shambat, and J. Vučković, "Photo-oxidative tuning of individual and coupled GaAs photonic crystal cavities," Opt. Express **22**(12), 15017–23 (2014).
23. A. R. A. Chalcraft, S. Lam, B. D. Jones, D. Szymanski, R. Oulton, A. C. T. Thijssen, M. S. Skolnick, D. M. Whittaker, T. F. Krauss, and A. M. Fox, "Mode structure of coupled L3 photonic crystal cavities," Opt. Express **19**(6), 5670–5675 (2011).
24. T. Cai, R. Bose, G. S. Solomon, and E. Waks, "Controlled coupling of photonic crystal cavities using photochromic tuning," Appl. Phys. Lett. **102**(14), 141118 (2013).
25. D. O'Brien, M. D. Settle, T. Karle, A. Michaeli, M. Salib, and T. F. Krauss, "Coupled photonic crystal heterostructure nanocavities," Opt. Express **15**(3), 1228–1233 (2007).
26. F. S. F. Brossard, B. P. L. Reid, C. C. S. Chan, X. L. Xu, J. P. Griffiths, D. A. Williams, R. Murray, and R. A. Taylor, "Confocal microphotoluminescence mapping of coupled and detuned states in photonic molecules," Opt. Express **21**(14), 16934–16945 (2013).
27. K. A. Atlasov, A. Rudra, B. Dwir, and E. Kapon, "Large mode splitting and lasing in optimally coupled photonic-crystal microcavities," Opt. Express **19**(3), 2619–2625 (2011).
28. K. H. Lee, A. M. Green, R. A. Taylor, D. N. Sharp, J. Scrimgeour, O. M. Roche, J. H. Na, A. F. Jarjour, A. J. Turberfield, F. S. F. Brossard, D. A. Williams, and G. A. D. Briggs, "Registration of single quantum dots using

Optics EXPRESS

cryogenic laser photolithography," Appl. Phys. Lett. **88**(19), 193106 (2006).
29. T. Yoshie, A. Scherer, J. Hendrickson, G. Khitrova, H. M. Gibbs, G. Rupper, C. Ell, O. B. Shchekin, and D. G. Deppe, "Vacuum Rabi splitting with a single quantum dot in a photonic crystal nanocavity," Nature **432**(7014), 200–203 (2004).
30. A. Badolato, K. Hennessy, M. Atatüre, J. Dreiser, E. Hu, P. M. Petroff, and A. Imamoğlu, "Deterministic Coupling of Single Quantum Dots to Single Nanocavity Modes," Science **308**(5275), 1158–1161 (2005).
31. L. P. Nuttall, F. S. F. Brossard, S. A. Lennon, B. P. L. Reid, J. Wu, J. Griffiths, and R. A. Taylor, "Optical fabrication and characterisation of SU-8 disk photonic waveguide heterostructure cavities," Opt. Express **25**(20), 24615–24622 (2017).
32. M. Notomi, "Manipulating light with strongly modulated photonic crystals," Reports Prog. Phys. **73**(9), 96501 (2010).
33. F. S. F. Brossard, V. Pecunia, A. J. Ramsay, J. P. Griffiths, M. Hugues, and H. Sirringhaus, "Inkjet-Printed Nanocavities on a Photonic Crystal Template," Adv. Mater. **29**(47), 1704425 (2017).
34. Lumerical Inc., http://www.lumerical.com/tcad-products/fdtd/.
35. D. C. Reynolds, K. K. Bajaj, C. W. Litton, G. Peters, P. W. Yu, and J. D. Parsons, "Refractive index, n, and dispersion, $-dn/d\lambda$, of GaAs at 2 K determined from Fabry-Perot cavity oscillations," J. Appl. Phys. **61**(1), 342 (1987).
36. T. C. Sum, A. A. Bettiol, J. A. van Kan, F. Watt, E. Y. B. Pun, and K. K. Tung, "Proton beam writing of low-loss polymer optical waveguides," Appl. Phys. Lett. **83**(9), 1707–1709 (2003).
37. Y. Tanaka, T. Asano, R. Hatsuta, and S. Noda, "Investigation of point-defect cavity formed in two-dimensional photonic crystal slab with one-sided dielectric cladding," Appl. Phys. Lett. **88**(1), 011112 (2006).
38. S. Tomljenovic-Hanic, C. M. de Sterke, M. J. Steel, B. J. Eggleton, Y. Tanaka, and S. Noda, "High-Q cavities in multilayer photonic crystal slabs," Opt. Express **15**(25), 17248–17253 (2007).
39. C. Cohen-Tannoudji, B. Diu, and F. Laloë, *Quantum Mechanics* (Wiley-Interscience, 1977), Chap. 4.